Stress-driven formation of terraced hollow oxide nanorods during metal oxidation

Guangwen Zhou[a)]
Department of Mechanical Engineering and Multidisciplinary Program of Materials Science and Engineering, State University of New York, Binghamton, New York 13902, USA

(Received 22 December 2008; accepted 17 March 2009; published online 18 May 2009)

We report the formation of terraced hollow Cu_2O nanorods upon oxidation of Cu(100) thin films at ~600 °C. Transmission electron microscopy and atomic force microscopy observations reveal that the oxide islands have an initially square pyramid shape that transits to an elongated nanorod shape and then to a terraced hollow nanorod morphology as the oxide growth proceeds. A mechanism based on the relaxation of interfacial epitaxial stress followed by the release of the bulk stress induced by the large volume expansion accompanying the conversion of metal into oxide is proposed to explain the pathway of the morphological evolution of this new oxide structure.
 [DOI: 10.1063/1.3118572]

I. INTRODUCTION

Oxidation of metals usually results in the generation of stresses in the oxide layer and the metal substrate.[1–4] A few major types of stresses can be categorized. The first type is epitaxial stresses arising from the epitaxial growth of initial oxide. The second is stresses resulting from the volume change that accompanies the conversion of metal into oxide. The other includes intrinsic growth stresses arising from the formation of new oxide phase within the already existing oxide, point defect stresses, and thermal-expansion mismatch stresses. The generation and relief of these stresses during the growth of bulk oxides have been extensively studied and it has been shown that the development of these stresses can often lead to fracture in the oxide scale and/or in the underlying metals, wrinkling of oxide films, or separation of the oxide-metal interface.[3,5–7] However, the mechanism governing the stress evolution during early stages of oxidation of metals is still to a significant degree unclear, this is largely due to the inability of traditional techniques to probe nanoscale oxide growth. In this work, we report a combined transmission electron microscopy (TEM) and atomic force microscopy (AFM) study of the early-stage oxidation of Cu(100), which reveals for the first time the complex interplay between oxide growth morphologies and various oxide growth stresses at the nanoscale. Specifically, our experimental observation suggests that the epitaxial stress generated in initially formed oxide islands can lead to a square-to-elongation shape transition of the oxide islands, while the volume expansion induced bulk stresses generated during subsequent growth stages of the oxide islands can be released by plastic sliding. We demonstrate that the generation and relaxation of these stresses during nanoscale oxidation of metals can be explored for creating novel oxide nanostructures.

We have chosen Cu as a model system in our study because Cu has been extensively studied as a prototypical system for understanding metal oxidation.[8–19] Meanwhile, Cuprous oxide (Cu_2O) has recently received much interest owing to its myriad technologically important applications such as solar energy conversion,[20,21] photocatalysts,[22] fuel cells,[23,24] emission control,[25,26] lithium ion batteries,[27] and gas sensors.[28] Moreover, Cu_2O is an ideal compound to study the effects of electron correlation on the electronic structure of transition metal compounds.[29] Nanostructured Cu_2O is expected to possess improved or unique properties compared to its bulk one and therefore much effort with majority using chemical synthesis techniques has been devoted to the production of Cu_2O nanostructures including nanoparticles,[30] nanowires,[31–33] nanotubes,[34] hollow spheres,[35,36] and nanocubes.[37,38] Herein we describe the formation of a new type of Cu_2O nanostructures, i.e., terraced hollow Cu_2O nanorods, via oxidation of Cu(100) thin films, where the oxide growth stresses associated with the oxidation of Cu (a_{Cu}=3.61 Å) into Cu_2O (a_{Cu_2O}=4.217 Å) play a critical role for the formation of this novel oxide structure.

II. EXPERIMENTAL DETAILS

Our oxidation experiments were carried out in a modified JEOL 200CX TEM.[39] This microscope is equipped with a high vacuum chamber with base pressure ~10^{-8} Torr. A controlled leak valve attached to the column permits the introduction of oxygen gas directly into the microscope to oxidize TEM samples. Cu(100) single crystal films with ~600 Å thickness were grown on irradiated NaCl(100) by sputter deposition. The metal films were removed from the substrate by flotation in de-ionized water, washed, and mounted on a specially prepared TEM specimen holder that allows for resistive heating to a maximum temperature of ~1000 °C. Any native Cu oxide is removed by annealing the films in the TEM under vacuum conditions at ~750 °C (Ref. 40) or by *in situ* annealing in methanol vapor at a pressure of 5×10^{-5} Torr but lower temperature (~350 °C), resulting in a clean copper surface.[41] Oxidation experiments were carried out at ~600 °C. After the Cu(100) films were oxidized continuously for ~30 min under an

[a)]Author to whom correspondence should be addressed. Electronic mail: gzhou@binghamton.edu.

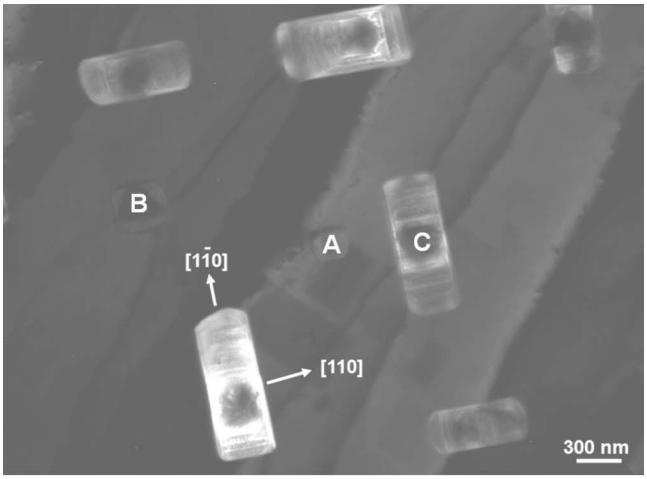

(a)

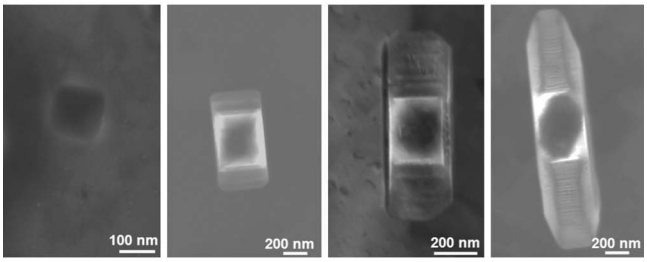

(b)

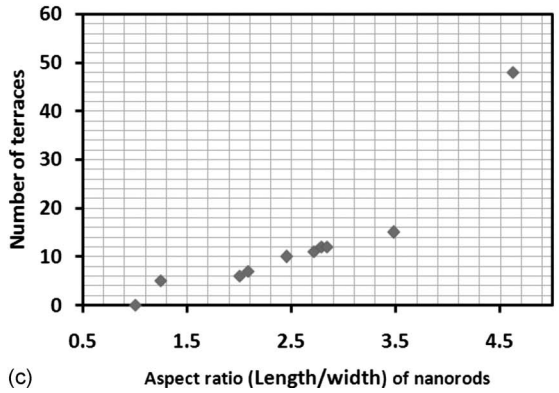

(c)

FIG. 1. (a) Typical morphology of Cu_2O terraced pyramids formed during oxidation of (001)Cu thin film (60 nm in thickness) at 600 °C in $pO_2=5\times10^{-4}$ Torr; (b) some Cu_2O islands with different length/width aspect ratios; (c) the correlation between the number of terraces and the island aspect ratio, as measured from different oxide islands.

oxygen partial pressure $(pO_2)=5\times10^{-4}$ Torr, the oxygen leaking was then stopped and the microscope column was quickly pumped to $\sim8\times10^{-8}$ Torr using the attached high vacuum pumps (turbo and ion pumps). The oxidized Cu films were first characterized by the *in situ* JEOL 200CX TEM, and then analyzed by electron diffraction (ED) and high resolution TEM (HRTEM) with a JEOL 2010 LaB6 operating at 200 keV. Thereafter, the surface morphology of the oxidized samples was further analyzed by AFM tapping mode at room temperature.

III. EXPERIMENTAL RESULTS

Figure 1(a) is a bright-field (BF) TEM image showing the morphology of typical Cu_2O islands formed on a Cu(100) surface, where the Cu film was oxidized for ~30 min at 600 °C in $pO_2=5\times10^{-4}$ Torr. These islands have square or elongated shape, and are roughly equally distributed along the two equivalent orientation pairs of the four crystallographic orientations, i.e., $\langle110\rangle$ and $\langle\bar{1}\bar{1}0\rangle$ or $\langle\bar{1}10\rangle$ and $\langle1\bar{1}0\rangle$. Small islands, as marked by *A* and *B*, have a square pyramid shape, while large ones, as marked by letter *C*, are nucleated at an earlier time than the small islands during the oxidation and have an elongated shape with terraces and ledges present on the island surfaces. The correlation between the island shape and size suggests that these different shapes (e.g., *A*-*C*) represent different island growth stages, i.e., the islands initially have a square shape, such as island *A*, and grow uniformly by keeping the square shape such as island *B*, and then transit to a rod shape which is accompanied by the formation of parallel terraces and ledges perpendicular to the elongation direction. This growth feature can be confirmed in Fig. 1(b), where oxide islands with different elongation lengths are shown. These images indicate that terraces and ledges do not occur in initially formed square-shaped islands. With continued oxidation, square islands become elongated and parallel terraces and ledges are formed along the elongation direction.

The number of terraces for different oxide islands is measured and its correlation with the island length/width aspect ratio is given in Fig. 1(c). It can be noted that the islands with a larger aspect ratio have more terraces. Since the island width is relatively constant, the correlation between the terrace number and the island aspect ratio suggests that the formation of terraces is closely related to the one-dimensional growth of the Cu_2O nanorods, i.e., more terraces are formed along the elongation direction as the one-dimensional oxide growth progresses. Here we want to emphasize that the elongation of the oxide islands as well as the dependence of the terrace number on the island aspect ratio [Fig. 1(c)] is unlikely due to the coalescence of square-shaped Cu_2O islands. This is because the width of each terrace along the elongation direction is much less than the edge length of square islands, as revealed in Figs. 1(a) and 1(b). Also, if the elongation of Cu_2O islands and their terrace formation are caused by island coalescence, then perfect alignment of square islands is needed. This is not the case because Cu_2O islands are nucleated randomly on Cu surfaces due to stochastic process of oxide nucleation during oxidation.[13]

ED is employed to determine the structure of the oxide phase as well as the orientation relationship between the metal and the oxide. Figure 2 shows the BF TEM image of one terraced oxide nanorod and the ED patterns from two different regions of the oxide island. The ED pattern (*A*) taken from the white square region *A* of the island can be indexed with Cu_2O structure. Since no Cu diffraction spots are present in the ED pattern (*A*), it can be easily inferred that the Cu film beneath the oxide island has completely been converted into Cu_2O in the region *A*. The ED pattern (*B*) is taken from the metal-oxide interface region as marked with the white square *B* and the pattern is composed of diffraction spots of both Cu and Cu_2O, suggesting the overlap

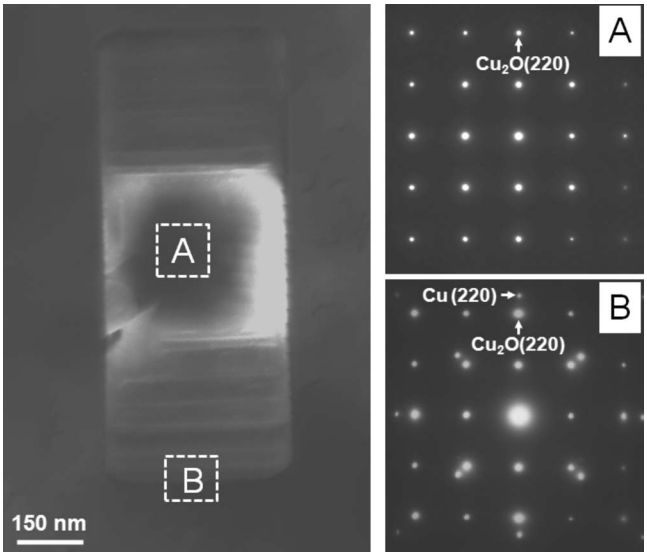

FIG. 2. Selected area ED pattern obtained from different positions of one terraced Cu_2O nanorod as shown by white squares: (a) from the center of the oxide island, (b) from the metal-oxide interface.

of Cu and Cu_2O lattices at the metal-oxide interface. The indexing of the ED pattern (*B*) reveals a cube-on-cube orientation relationship of the metal and oxide, i.e., $Cu_2O(220)\|Cu(220)$, at their interface region.

HRTEM examinations were carried out to investigate the microstructure of these terraced nanorods, especially at the metal-oxide interface, which provide insight into the growth mechanism of these oxide nanorods. Figure 3(a) shows the BF image of one Cu_2O terraced nanorod and an HRTEM image from the metal-oxide interface region marked by the white rectangle. Moiré fringes are visible at the interface area owing to the overlap of Cu and Cu_2O lattices near the island edge. The occurrence of moiré fringes only at the interface area further confirms the above ED analysis that the oxide island has completely penetrated through the Cu film. Figure 3(b) is a schematic illustration of the shape of the metal-oxide interface (*ABCD*). The width (~23 nm) of the $Cu-Cu_2O$ overlap zone is determined by measuring the width of the region with moiré fringes. The HREM image reveals that Cu lattice appears undistorted while Cu_2O lattice has a lot of distortions near the interface. The Cu_2O lattice in the region as far as 20 nm away from the interface shows a relatively intact structure. These structure features of the Cu and Cu_2O lattices suggest that Cu lattice is relatively stress free while the Cu_2O lattice near the metal-oxide interface is highly stressed.

In order to obtain more details about the three-dimensional (3D) structure of these terraced oxide nanorods, AFM is employed to examine the surface topology of oxidized Cu(100) thin films. Figure 4(a) shows the AFM image of one terraced oxide nanorod, where the island height is ~80 nm above the Cu surface and terraces/ledges are present on the island surface. Figure 4(b) is the AFM image of a terraced oxide island viewed from the opposite perspective as compared to the situation in acquiring the AFM image in Fig. 4(a). The surface topology obtained from Fig. 4(b) reveals that these terraced nanorods have a hollow structure

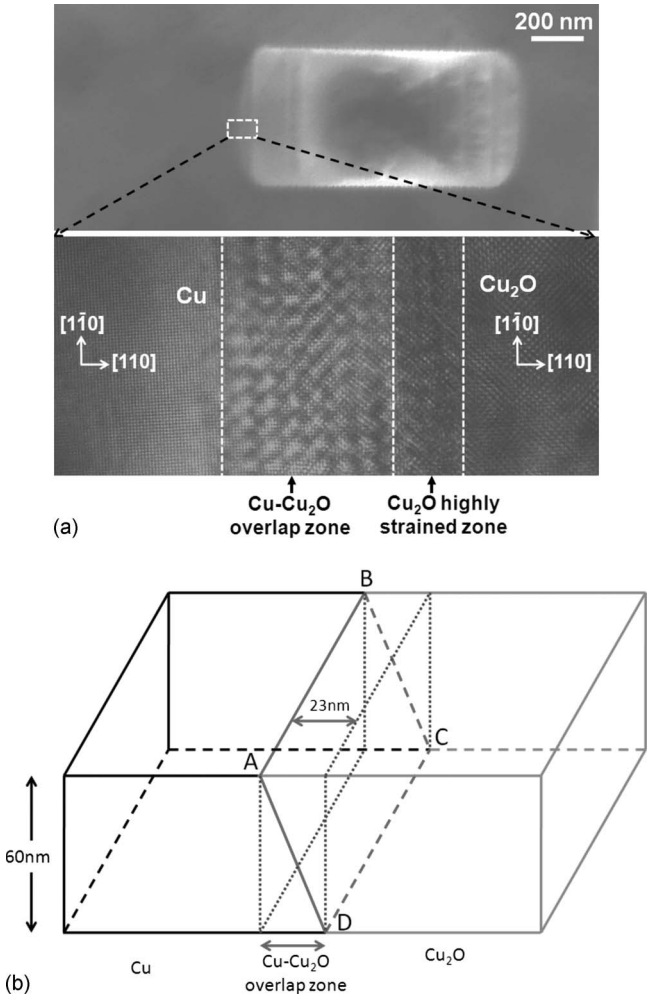

FIG. 3. (a) HRTEM analysis of the microstructure at the Cu/Cu_2O interface: BF micrograph of one terraced Cu_2O nanorod and the HRTEM image from the Cu_2O-Cu interface area shown by the white rectangle, where moiré fringes are visible at the interface area owing to the lattice overlap of Cu and Cu_2O. The Cu_2O phase near the metal-oxide interface shows large lattice distortion due to the growth stress generated by the large volume expansion from Cu to Cu_2O, while the Cu_2O lattice in the region ~20 nm away from the interface shows relatively intact structure. (b) Schematic illustration of the inclined Cu_2O-Cu interface (*ABCD*), where the width (~23 nm) of the $Cu-Cu_2O$ overlap zone is obtained by measuring the width of the interface region with moiré fringes.

(like a surface pit) and terraces/ledges are present along the inner walls of the pit. The total depth of the terraced oxide pit is about 128 nm below the Cu surface, which is larger than the original thickness (~60 nm) of unoxidized Cu films. Based on these TEM and AFM observations, we have proposed a 3D shape of these terraced hollow Cu_2O nanorods, which is schematically shown in Fig. 4(c).

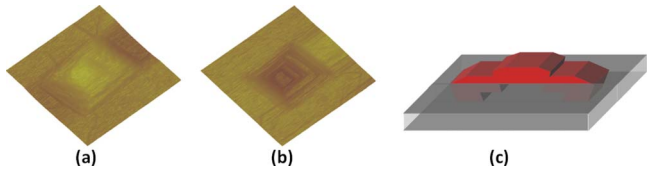

FIG. 4. (Color online) AFM images of terraced hollow Cu_2O nanorods viewed from different perspectives: (a) top-down perspective, (b) bottom-up perspective (2×2 μm^2, *z* range: 0.6 μm); (c) proposed 3D shape of terraced hollow nanorods, note that the oxide island has completely penetrated through the Cu film.

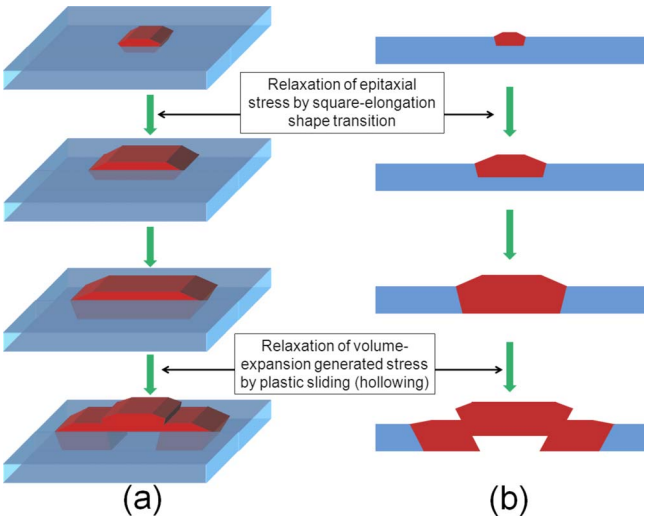

FIG. 5. (Color online) Proposed stress-relaxation mechanism for the formation of terraced hollow oxide nanorods during Cu(100) oxidation, (a) 3D view and (b) side view. The elongation of initially square-shape Cu_2O islands is driven by relaxation of the epitaxial stress at the metal-oxide interface, and the island hollowing is related to the process of plastic sliding to release the compressive stress generated by the large volume expansion accompanying the conversion of Cu into Cu_2O during the oxidation.

IV. DISCUSSION

Two questions are raised from our TEM and AFM observations of these terraced hollow Cu_2O nanorods: (1) Why the oxide islands become elongated from their initially square pyramid shape? (2) How terrace/ledge formation and hollowing occur during the elongation of the oxide islands? To address these questions, we start by describing the growth process of oxide islands during metal oxidation and consider the effect of various growth stresses associated with the oxide formation on the shape evolution of oxide islands. Figure 5 is the proposed mechanism showing the formation of the terraced hollow Cu_2O nanorods, where the island elongation is driven by relaxation of the epitaxial stress, which is followed by the island hollowing driven by relaxation of the geometrically induced growth stress due to the large volume expansion accompanying the conversion of Cu into Cu_2O.

The initially formed oxide islands are epitaxial with the Cu substrate, as known from the above ED analysis. Owing to their large lattice mismatch between Cu and Cu_2O, epitaxial stress is generated in initially formed Cu_2O islands. Since stressed islands are inherently unstable and have to relax, the relaxation of the epitaxial stress often leads to island shape transition. Tersoff and Tromp[42] developed an analytical model and showed that strained epitaxial islands, as they grow in size, may undergo the shape transition: Below a critical size, islands have a compact shape, however, at a larger size, they adopt a long thin shape, which has an energy minimum for the system because of the tradeoff between the increase in surface/interfacial energies and reduction in the epitaxial strain energy. Since the Cu_2O islands formed during Cu(100) oxidation are epitaxial with the Cu substrate, the observed shape transition from initially square shape to elongation is a typical phenomenon driven by the elastic strain relief: elongated shape allows better elastic relaxation of the epitaxial stress when the islands grow to a larger size.[43]

It has been previously revealed that the oxidation of Cu thin films results in 3D growth of oxide islands,[44,45] i.e., the oxide islands are embedded into the Cu substrate as growth proceeds, although the embedding rate is much slower than the lateral growth. This 3D growth feature is also confirmed by thermal reduction of oxide islands formed on Cu(100) surfaces, which leads to the formation of nanopits at the sites which are originally occupied by oxide islands.[40,46] During initial stages of Cu oxidation, the oxide islands have a shallow embedment just below the Cu surface and the stress in oxide islands is therefore dominated by the epitaxial stress due to lattice mismatch between Cu_2O and Cu. This epitaxial stress becomes the driving force for the elongation of initially square-shaped oxide islands. However, since the Cu film is oxidized continuously, the oxide islands can grow deeper into the Cu film and eventually penetrates through the Cu thin film. This will create huge compressive stress in the oxide island due to the large volume expansion (~60%) associated with the conversion of Cu into Cu_2O. This compressive stress first causes lattice distortions in the oxide, which can be discerned from the HREM image shown in Fig. 3(a). With the continuous formation of new Cu_2O at the metal-oxide interface, this volume expansion induced stress increases progressively, and finally causes plastic sliding inside the oxide island to release the compressive stress. As a result, the central part of the island is squeezed out, leading to the island hollowing and formation of terraces ledges along the sliding planes. The relaxation of the volume stress by island sliding also leads to the restoration of distorted Cu_2O lattices to their normal structure. This can be noticed from the HRTEM image in Fig. 3, where the Cu_2O lattices far away from the metal-oxide interface show very few distortions because the stress in these oxide regions is already released by the sliding. This process of buildup of the compressive stress by progressive oxide growth at the metal-oxide interface and release of the stress by island sliding can repeats itself during the oxidation, which leads to the formation of hollow nanorods with multiple terraces and ledges. Since oxide islands have much faster growth rate along one direction (i.e., the elongation direction), the buildup of the compressive stress along this elongation direction is thus much faster than the other direction. As a result, multiple parallel terraces/ledges are formed along the elongation direction, while very few terraces/ledges are observed along the island width direction because of the much slower growth rate along this direction. These growth features can be noted in Figs. 1 and 2.

Clearly, the hollowing process of Cu_2O nanorods during the oxidation of Cu films depends on the mechanical properties of the oxide phase and the metal films. Cu_2O has a smaller Young's modulus (E) and shear modulus (G) than Cu (i.e., $E_{Cu_2O} \sim 30$ GPa, $G_{Cu_2O} \sim 10$ GPa, $E_{Cu} \sim 124$ GPa, and $G_{Cu} \sim 40$ GPa), even considering their temperature dependence.[47] Also, any pre-existing dislocations in the Cu thin films can be eliminated by annealing the films at ~900 °C prior to the oxidation experiments at the lower temperature (600 °C). This feature of dislocation free in the Cu film around the oxide islands can be verified from our HRTEM observations, as shown in Fig. 3(a). These two factors, i.e., the higher mechanical modulus of Cu than Cu_2O

and the absence of pre-existing dislocations in the Cu film surrounding the oxide islands, drive the oxide nanorods to release the compressive stress rather than by the adjacent Cu thin film.

According to this analysis, we anticipate that the appropriate choice of experimental parameters is critical for the formation of these terraced hollow Cu_2O nanorods. For instance, if a thicker Cu film is oxidized, a longer oxidation time is needed for oxide islands completely penetrating through the oxidizing Cu film, which correspondingly delays the formation of terraced hollow Cu_2O nanorods. This speculation is consistent with our previous observation on the elongation processes of Cu_2O islands during the oxidation of thicker Cu(100) films (~700 Å), where no terraced hollow oxide nanorods were observed for oxidation at 600 °C for more than 20 min.[43] Another important factor controlling the formation of this terraced hollow nanorod structure is oxidation temperature. For example, if a Cu film is oxidized at a temperature well above 600 °C, the growth rate of oxide islands shall be much faster due to the enhanced surface and bulk diffusion of the reactants. Therefore, the initially square-shaped oxide islands can quickly penetrate through the oxidizing Cu film well before the epitaxial stress taking effect for the square-to-elongation shape transition. This can lead to the formation of square-shaped hollow terraced oxide pyramids. This is confirmed from our earlier experiments on the oxidation of Cu(100) thin films at 900 °C, where only square-shaped terraced hollow Cu_2O pyramids were observed.[48] Therefore, the formation of this terraced hollow nanorod structure requires the appropriate choice of experimental conditions including the thickness of oxidizing metal thin films and oxidation temperature, which accommodate the sequential relaxation of the epitaxial stress and the subsequent bulk stress induced by the large volume expansion accompanying the conversion of Cu into Cu_2O.

V. CONCLUSIONS

In summary, we report the formation of terraced hollow Cu_2O nanorods during early stages of oxidation of Cu(100) thin films at 600 °C. A mechanism based on the sequential relaxation of the epitaxial stress due to the metal-oxide lattice mismatch and the bulk stress caused by the volume expansion accompanying the conversion of metal into oxide is proposed to describe the formation of this peculiar oxide nanostructure. Island formation during metal oxidation has been observed in many other metal systems, such as Ni, Fe, Ti, Co, Pd, Ir, Sn, as well as in Cu.[43,49–52] By carefully choosing the oxidation conditions such as oxidation temperature, thickness of metal thin films, it is reasonable to expect that similar terraced hollow oxide nanorods can be realized in these metal systems. These terraced hollow nanorods possess exposed surfaces of both the outer and inner walls and therefore have larger exposed surface-to-volume ratio compared to other forms of nanostructures. Such oxide nanostructures with highly increased reactive surface area may find technological applications such as catalysis, energy conversion, and sensors.

ACKNOWLEDGMENTS

The author is grateful to Professor Judith C Yang for help and advice for the performance of this work. The author gratefully acknowledges support from the National Science Foundation (NSF) under the Grant No. CMMI-0825737.

[1] H. E. Evans, Int. Mater. Rev. **40**, 1 (1995).
[2] P. Hancock and R. C. Hurst, in *Advances in Corrosion Science and Technology*, edited by R. W. Staehle and M. G. Fontana (Plenum, New York, 1974), p. 1.
[3] N. Birks, G. H. Meier, and F. S. Pettit, *Introduction to High Temperature Oxidation of Metals* (Cambridge University Press, Cambridge, 2006).
[4] B. W. Veal, A. P. Paulikas, and P. Y. Hou, Nature Mater. **5**, 349 (2006).
[5] P. Y. Hou and K. Priimak, Oxid. Met. **63**, 113 (2005).
[6] V. K. Tolpygo and D. R. Clarke, Acta Mater. **46**, 5153 (1998).
[7] Z. G. Yang and P. Y. Hou, Mater. Sci. Eng., A **391**, 1 (2005).
[8] J. C. Yang, B. Kolasa, J. M. Gibson, and M. Yeadon, Appl. Phys. Lett. **73**, 2841 (1998).
[9] J. C. Yang, D. Evan, and L. Tropia, Appl. Phys. Lett. **81**, 241 (2002).
[10] K. R. Lawless and A. T. Gwathmey, Acta Metall. **4**, 153 (1956).
[11] S. Ronnquist and H. Fisher, J. Inst. Met. **89**, 65 (1960).
[12] R. H. Milne and A. Howie, Philos. Mag. A **49**, 665 (1984).
[13] J. C. Yang, M. Yeadon, B. Kolasa, and J. M. Gibson, Scr. Mater. **38**, 1237 (1998).
[14] J.-H. Park and K. Natesan, Oxid. Met. **39**, 411 (1993).
[15] Y. Zhu, K. Mimura, and M. Isshiki, Oxid. Met. **62**, 207 (2004).
[16] R. Haugsrud, J. Electrochem. Soc. **149**, B14 (2002).
[17] J. Li, J. W. Mayer, and E. G. Colgan, J. Appl. Phys. **70**, 2820 (1991).
[18] S. Mrowec and A. Stokosa, Oxid. Met. **3**, 291 (1971).
[19] J. Li, G. Vizkelethy, P. Revesz, J. W. Mayer, and K. N. Tu, J. Appl. Phys. **69**, 1020 (1991).
[20] A. O. Musa, T. Akomolafe, and M. J. Carter, Sol. Energy Mater. Sol. Cells **51**, 305 (1998).
[21] C. A. N. Fernando, P. H. C. de Silva, S. K. Wethasinha, I. M. Dharmadasa, T. Delsol, and M. C. Simmonds, Renewable Energy **26**, 521 (2002).
[22] W. Siripala, A. Ivanovskaya, T. F. Jaramillo, S. H. Baeck, and E. W. McFarland, Sol. Energy Mater. Sol. Cells **77**, 229 (2003).
[23] L. Zhou, S. Gunther, D. Moszynski, and R. Imbihl, J. Catal. **235**, 359 (2005).
[24] X. Q. Wang, J. A. Rodriguez, J. C. Hanson, D. Gamarra, A. Martinez-Arias, and M. Fernandez-Garcia, J. Phys. Chem. B **109**, 19595 (2005).
[25] J. B. Wang, D. H. Tsai, and T. J. Huang, J. Catal. **208**, 370 (2002).
[26] W. Liu and M. Flytzani-stephanopoulos, J. Catal. **153**, 317 (1995).
[27] P. Poizot, S. Laruelle, S. Grugeon, L. Dupont, and J.-M. Tarascon, Nature (London) **407**, 496 (2000).
[28] S. T. Shishiyanu, T. S. Shishiyanu, and O. L. Lupan, Sens. Actuators B **113**, 468 (2006).
[29] D. Snoke, Science **298**, 1368 (2002).
[30] M. Yin, C. K. Wu, Y. B. Lou, C. Burda, J. T. Koberstein, Y. M. Zhu, and S. O'Brien, J. Am. Chem. Soc. **127**, 9506 (2005).
[31] W. Z. Wang, O. K. Varghese, C. M. Ruan, M. Paulose, and C. A. Grimes, J. Mater. Res. **18**, 2756 (2003).
[32] W. Z. Wang, G. H. Wang, X. S. Wang, Y. J. Zhan, Y. K. Liu, and C. L. Zheng, Adv. Mater. (Weinheim, Ger.) **14**, 67 (2002).
[33] X. C. Jiang, T. Herricks, and Y. N. Xia, Nano Lett. **2**, 1333 (2002).
[34] M. H. Cao, C. W. Hu, Y. H. Wang, Y. H. Guo, C. X. Guo, and E. B. Wang, Chem. Commun. (Cambridge) **15**, 1884 (2003).
[35] Y. Chang, J. J. Teo, and H. C. Zeng, Langmuir **21**, 1074 (2005).
[36] M. Yang and J. J. Zhu, J. Cryst. Growth **256**, 134 (2003).
[37] L. F. Gou and C. J. Murphy, Nano Lett. **3**, 231 (2003).
[38] M. H. Kim, B. Lim, E. P. Lee, and Y. N. Xia, J. Mater. Chem. **18**, 4069 (2008).
[39] M. L. McDonald, J. M. Gibson, and F. C. Unterwald, Rev. Sci. Instrum. **60**, 700 (1989).
[40] G. W. Zhou and J. C. Yang, Phys. Rev. Lett. **93**, 226101 (2004).
[41] S. M. Francis, F. M. Leibsle, S. Haq, N. Xiang, and M. Bowker, Surf. Sci. **315**, 284 (1994).
[42] J. Tersoff and R. M. Tromp, Phys. Rev. Lett. **70**, 2782 (1993).
[43] G. W. Zhou and J. C. Yang, Phys. Rev. Lett. **89**, 106101 (2002).
[44] J. C. Yang, M. Yeadon, B. Kolasa, and J. M. Gibson, Appl. Phys. Lett. **70**, 3522 (1997).
[45] G. W. Zhou and J. C. Yang, Appl. Surf. Sci. **222**, 357 (2004).

[46]G. W. Zhou, W. Dai, and J. C. Yang, Phys. Rev. B **77**, 245427 (2008).
[47]H. J. Frost and M. F. Ashby, *Deformation-Mechanism Maps* (Pergamon, Oxford, 1982).
[48]G. W. Zhou, W. S. Slaughter, and J. C. Yang, Phys. Rev. Lett. **94**, 246101 (2005).
[49]K. Thurmer, E. Williams, and J. Reutt-Robey, Science **297**, 2033 (2002).
[50]S. Aggarwal, A. P. Monga, S. R. Perusse, R. Ramesh, V. Ballarotto, E. D. Williams, B. R. Chalamala, Y. Wei, and R. H. Reuss, Science **287**, 2235 (2000).
[51]S. Aggarwal, S. B. Ogale, C. S. Ganpule, S. R. Shinde, V. A. Novikov, A. P. Monga, M. R. Burr, R. Ramesh, V. Ballarotto, and E. D. Williams, Appl. Phys. Lett. **78**, 1442 (2001).
[52]E. E. Hajcsar, P. R. Underhill, and W. W. Smeltzer, Langmuir **11**, 4862 (1995).